SUB-NYQUIST PULSE DOPPLER MIMO RADAR

David Cohen, Deborah Cohen, Yonina C. Eldar

Technion - Israel Institute of Technology
Haifa, Israel
{davidco@campus, debby@campus, yonina@ee}.technion.ac.il

Alexander M. Haimovich

New Jersey Institute of Technology
New Jersey, USA
haimovic@njit.edu

ABSTRACT

Pulse Doppler multiple input multiple output (MIMO) radar allows to simultaneously detect targets' range, azimuth and velocity. Achieving high resolution requires a large number of transmit and receive antennas, as well as high sampling rates leading to a torrent of samples. Overcoming the rate bottleneck, sub-Nyquist sampling methods have been proposed that break the link between single antenna radar signal bandwidth and range resolution. In this work, we present a sub-Nyquist MIMO radar (SUMMeR) system that extends these methods to a multiple antenna setting. We apply the Xampling framework both in time and space, thus reducing both the number of deployed antennas and samples per receiver, without degrading time and spatial resolution, as illustrated in the simulations.

Index Terms— MIMO radar, sub-Nyquist sampling, compressed sensing

I. INTRODUCTION

Multiple input multiple output (MIMO) radar is an emerging technology [1] that has significant potential for advancing state-of-the-art modern radar. MIMO radar combines multiple antenna elements at the transmitter and receiver where each transmitter radiates a different waveform. In this paper, we focus on the collocated MIMO architecture [2], in which the elements are close to each other.

Collocated MIMO radar systems exploit waveform diversity, based on mutual orthogonality of the transmitted signals [3]. This generates a virtual array induced by the phase differences between transmit and receive antennas. Such systems thus achieve higher resolution than their phased-array counterpart with the same number of elements. This increased performance comes at the cost of high complexity in terms of transmitters and receivers design as well as heavy computational load. Several works have thus considered exploiting the sparse nature of the targets scene to reduce the number of antenna elements and samples per receiver while preserving range, azimuth and Doppler resolution.

The partial problem of azimuth recovery of targets all in the same range-Doppler bin is investigated in [4]. There, spatial compression is performed, where the number of antennas is reduced while preserving the azimuth resolution. Beamforming is applied on the time domain samples obtained from the thinned array at the Nyquist rate and the azimuths are recovered using compressed sensing (CS) techniques. In [5], [6], [7], a time compression approach is adopted where the Nyquist samples are compressed in each antenna before being forwarded to the central unit. While [5] exploits sparsity and uses CS recovery methods, [6], [7] apply matrix completion techniques to recover the missing samples, prior to azimuth-Doppler [6] or range-azimuth-Doppler [7] reconstruction. However, the authors do not address sampling and processing rate reduction since the compression is performed in the digital domain, after sampling, and the missing samples are reconstructed before recovering the targets parameters.

In all the above works, recovery is performed in the time domain on acquired or recovered Nyquist rate samples for each antenna. To reduce the sampling rate while preserving the range resolution, the authors in [8] consider frequency domain recovery. The work of [8] demonstrates low-rate range-Doppler recovery for a single antenna, including sub-Nyquist acquisition digital processing. Low-rate data acquisition is based on the ideas of Xampling [9], which obtains Fourier coefficients of the received signal from sub-Nyquist samples and recovers the targets range-Doppler map from these. A practical analog front-end implementing such a sampling scheme is presented in [10].

The work of [8] exploits the Xampling framework to break the link between radar signal bandwidth and sampling rate, which defines the time or range resolution. Here, we present the sub-Nyquist MIMO radar (SUMMeR) system, that extends this concept in the context of MIMO radar to break the link between the aperture and the number of antennas, which defines the spatial or azimuth resolution. We consider azimuth-range-Doppler recovery and apply the concept of Xampling both in space (antennas deployment) and in time (sampling scheme) in order to simultaneously reduce the required number of antennas and samples per receiver, without degrading time and spatial resolution. To this end, we express the "Xamples", or compressed samples, both in time and space, in terms of the targets unknown parameters, namely range, azimuth and Doppler, and show how these can be recovered efficiently from the sub-Nyquist samples. We also derive necessary conditions on the minimal number of samples and antennas for perfect recovery of the azimuth-range-Doppler map in noiseless settings and show that these depend only on the maximal number of targets to be detected. Simulations demonstrate that SUMMeR preserves time an spatial resolution with respect to classic Nyquist MIMO.

This paper is organized as follows. In Section II, we describe the MIMO signal model and SUMMeR system. Section III introduces our sub-Nyquist sampling scheme and azimuth-range-Doppler recovery algorithm. Numerical experiments are presented in Section IV.

II. MIMO RADAR MODEL

II-A. SUMMeR architecture

The traditional approach to collocated MIMO adopts a virtual ULA structure [11], where R receivers, spaced by $\frac{\lambda}{2}$ and T transmitters, spaced by $R\frac{\lambda}{2}$ (or vice versa), form two ULAs. Here, λ is the signal wavelength. Coherent processing of the resulting TR channels generates a virtual array equivalent to a phased array with TR $\frac{\lambda}{2}$-spaced receivers and normalized aperture $Z = \frac{TR}{2}$. This standard array structure and the corresponding receiver virtual array are illustrated in Fig. 1(a)-(b) for $R = 3$ and $T = 5$. The blue circles represent the receivers and the red squares are the transmitters.

Each transmitting antenna sends P pulses, such that the mth

This work was funded by the European Union's Horizon 2020 research and innovation program under grant agreement ERC-BNYQ, and by the Israel Science Foundation under Grant no. 335/14. Deborah Cohen is grateful to the Azrieli Foundation for the award of an Azrieli Fellowship.

transmitted signal is given by

$$s_m(t) = \sum_{p=0}^{P-1} h_m\left(t - p\tau\right) e^{j2\pi f_c t}, \quad 0 \le t \le P\tau, \tag{1}$$

where $h_m\left(t\right), 0 \le m \le T-1$ are narrowband and orthogonal pulses with bandwidth B_h, modulated with carrier frequency f_c. The coherent processing interval (CPI) is equal to $P\tau$, where τ denotes the pulse repetition interval (PRI). For convenience, we assume that $f_c\tau$ is an integer, so that the delay $e^{-j2\pi f_c \tau p}$ is canceled in the modulation [12]. The pulse time support is denoted by T_p.

MIMO radar architectures impose several requirements on the transmitted waveform family. Besides traditional demands from radar waveforms such as low sidelobes, MIMO transmit antennas rely on orthogonal waveforms. In addition, to avoid cross talk between the T signals and form TR channels, the orthogonality condition should be invariant to time shifts, that is $\int_{-\infty}^{\infty} s_i\left(t\right) s_j^*\left(t-\tau_0\right) dt = \delta\left(i-j\right)$, for $i, j \in [0, M-1]$ and for all τ_0. This property implies that the orthogonal signals cannot overlap in frequency [13], leading to frequency division multiple access (FDMA). Alternatively, time invariant orthogonality can be approximately achieved using code division multiple access (CDMA). In this work, we employ FMDA waveforms and for simplicity, $\{h_m(t)\}_{m=0}^{T-1}$ are frequency-shifted versions of a low-pass pulse $h_0(t)$ whose Fourier transform $H_0\left(\omega\right)$ has bandwidth B_h, such that

$$H_m\left(\omega\right) = H_0\left(\omega - 2\pi f_m\right). \tag{2}$$

Consider L non-fluctuating point-targets, according to the Swerling-0 model [14]. Each target is identified by its parameters: radar cross section (RCS) $\tilde{\alpha}_l$, distance between the target and the array origin or range R_l, velocity v_l and azimuth angle relative to the array θ_l. Our goal is to recover the targets' delay $\tau_l = \frac{2R_l}{c}$, azimuth sinus $\vartheta_l = \sin(\theta_l)$ and Doppler shift $f_l^D = \frac{2v_l}{c} f_c$ from the received signals. The targets are assumed to be stationary and the transmitted waveforms are narrowband. These traditional MIMO assumptions ensure constant α_l, τ_l, θ_l and f_l^D over the channels and during the CPI (see [15] for more details).

The SUMMeR system implements compression in both space and time, reducing the number of antennas as well as the number of samples acquired by each receiver, while preserving range and azimuth resolution. We begin by describing the spatial compression. Time compression is introduced in Section III.

Consider a collocated MIMO radar system with $M < T$ transmit antennas and $Q < R$ receive antennas, whose locations are chosen uniformly at random within the aperture of the virtual array described above, that is $\{\xi_m\}_{m=0}^{M-1} \sim \mathcal{U}\left[0, Z\right]$ and $\{\zeta_q\}_{q=0}^{Q-1} \sim \mathcal{U}\left[0, Z\right]$, respectively. Note that, in principle, the antenna locations can be chosen on the ULAs' grid. However, this configuration is less robust to range-azimuth ambiguity and leads to coupling between these parameters in the presence of noise, as shown in [15]. In Section III, we present lower bounds on the number of antennas M and Q. The spatially thinned array structure is illustrated in Fig. 1(c), for $Q = 2$ and $M = 3$.

Since we adopt a FDMA framework, spatial compression, which in particular reduces the number of transmit antennas, removes the corresponding transmitting frequency bands as well. The transmitted signals are illustrated in Fig. 2 in the frequency domain. Figure 2(a) and (b) show a standard FDMA transmission for $T = 5$ and the resulting signal after spatial compression for $M = 3$.

II-B. Received Signal

The transmitted pulses are reflected by the targets and collected at the receive antennas. Under the assumptions described above, the

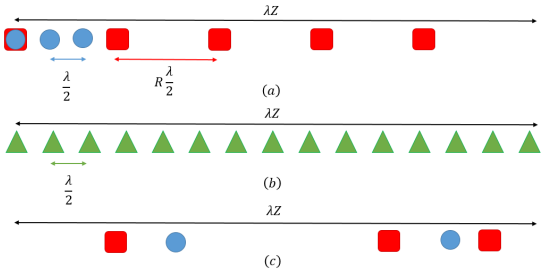

Fig. 1. Illustration of MIMO arrays: (a) standard array, (b) virtual array, (c) thinned array.

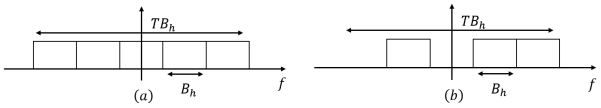

Fig. 2. FDMA transmissions: (a) standard, (b) spatial compression.

received signal $\tilde{x}_q(t)$ at the qth antenna is then a sum of time-delayed, scaled replica of the transmitted signals:

$$\tilde{x}_q\left(t\right) = \sum_{m=0}^{T-1} \sum_{l=1}^{L} \tilde{\alpha}_l s_m\left(\frac{c+v_l}{c-v_l}\left(t - \frac{R_{l,mq}}{c+v_l}\right)\right), \tag{3}$$

where $R_{l,mq} = 2R_l - \left(R_{lm} + R_{lq}\right)$, with $R_{lm} = \lambda\xi_m\vartheta_l$ and $R_{lq} = \lambda\zeta_q\vartheta_l$ accounting for the array geometry, as illustrated in Fig. 3. The received signal at the qth antenna is further simplified and after

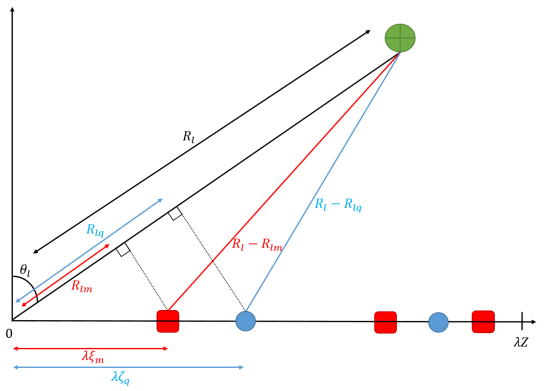

Fig. 3. MIMO array configuration.

demodulation to baseband is given by

$$x_q\left(t\right) = \sum_{p=0}^{P-1} \sum_{m=0}^{M-1} \sum_{l=1}^{L} \alpha_l h_m\left(t - p\tau - \tau_l\right) e^{j2\pi\beta_{mq}\vartheta_l} e^{j2\pi f_l^D p\tau}, \tag{4}$$

where $\beta_{mq} = \left(\zeta_q + \xi_m\right)\left(f_m \frac{\lambda}{c} + 1\right)$. It will be convenient to express $x_q(t)$ as a sum of single frames

$$x_q(t) = \sum_{p=0}^{P-1} x_q^p(t), \tag{5}$$

where

$$x_q^p(t) = \sum_{m=0}^{M-1} \sum_{l=1}^{L} \alpha_l h(t - \tau_l - p\tau) e^{j2\pi\beta_{mq}\vartheta_l} e^{j2\pi f_l^D p\tau}. \tag{6}$$

Our goal is to estimate the targets range, azimuth and velocity, i.e. to estimate τ_l, ϑ_l and f_l^D from low rate samples of $x_q(t)$, and a small number M and Q of antennas.

III. SUB-NYQUIST RANGE-AZIMUTH-DOPPLER RECOVERY

In this section, we describe how the range-azimuth-Doppler map can be recovered from Xamples in time and space and formulate necessary conditions on the number of channels, samples per receiver and pulses per transmitter to allow for perfect recovery in noiseless settings. We next present our range-azimuth-Doppler recovery algorithm based on the concept of Doppler focusing introduced in [8].

The received signal $x_q^p(t)$ at the qth antenna is limited to $t \in [p\tau,(p+1)\tau]$ and thus can be represented by its Fourier series

$$x_q^p(t) = \sum_{k\in\mathbb{Z}} c_q^p[k]\, e^{-j2\pi kt/\tau}, \quad t\in[p\tau,(p+1)\tau], \tag{7}$$

where, for $-\frac{NT}{2} \le k \le \frac{NT}{2}-1$, with $N=\tau B_h$,

$$c_q^p[k] = \frac{1}{\tau}\sum_{m=0}^{M-1}\sum_{l=1}^{L}\alpha_l e^{j2\pi\beta_{mq}\vartheta_l} e^{-j\frac{2\pi}{\tau}k\tau_l} e^{j2\pi f_l^D p\tau} H_m\left(\frac{2\pi}{\tau}k\right). \tag{8}$$

We observe that the unknown parameters τ_l, ϑ_l and f_l^D are embodied in these coefficients.

To obtain the Fourier coefficients $c_q^p[k]$ in (8) from low-rate samples of the received signal $x_q^p(t)$, we use the sub-Nyquist sampling scheme presented in [8], [10]. For each received transmission, Xampling allows one to obtain an arbitrary set κ, comprised of $K=|\kappa|$ frequency components from K point-wise samples of $x_q^p(t)$ after appropriate analog preprocessing. Therefore, MK Fourier coefficients are acquired at each receiver for each pulse from MK samples, with K coefficients per frequency band or transmission.

After separation to channels by matched filtering, the normalized and aligned Fourier coefficients $y_{m,q}^p[k] = \frac{\tau}{|H_0(\frac{2\pi}{\tau}k)|^2}\tilde{c}_{q,m}^p[k+f_m\tau]$, with $\tilde{c}_{q,m}^p[k] = c_q^p[k]\,H_m^*\left(\frac{2\pi}{\tau}k\right)$, are given by

$$y_{m,q}^p[k] = \sum_{l=1}^{L}\alpha_l e^{j2\pi\beta_{mq}\vartheta_l} e^{-j\frac{2\pi}{\tau}k\tau_l} e^{-j2\pi f_m\tau_l} e^{j2\pi f_l^D p\tau}, \tag{9}$$

for $-\frac{N}{2}\le k\le\frac{N}{2}-1$.

III-A. Range-Azimuth-Doppler Recovery Conditions

As in traditional MIMO, assume that the time delays, azimuths and Doppler frequencies are aligned to a grid. In particular, $\tau_l = \frac{\tau}{TN}s_l$, $\vartheta_l = -1+\frac{2}{TR}r_l$ and $f_l^D = -\frac{1}{2\tau}+\frac{1}{P\tau}u_l$, where s_l, r_l and u_l are integers satisfying $0\le s_l\le TN-1$, $0\le r_l\le TR-1$ and $0\le u_l\le P-1$, respectively. Let $\mathbf{Z}^m$ be the $KQ\times P$ matrix with qth column given by the vertical concatenation of $y_{m,q}^p[k], k\in\kappa$, for $0\le q\le Q-1$. We can then write $\mathbf{Z}^m$ as

$$\mathbf{Z}^m = \left(\bar{\mathbf{B}}^m\otimes\mathbf{A}^m\right)\mathbf{X}_D\mathbf{F}^H. \tag{10}$$

Here, $\mathbf{A}^m$ denotes the $K\times TN$ matrix whose (k,n)th element is $e^{-j\frac{2\pi}{TN}\kappa_k n}e^{-j2\pi\frac{f_m}{B_h}\frac{n}{T}}$ with κ_k the kth element in κ, $\mathbf{B}^m$ is the $Q\times TR$ matrix with (q,p)th element $e^{-j2\pi\beta_{mq}(-1+\frac{2}{TR}p)}$ and and $\mathbf{F}$ denotes the $P\times P$ Fourier matrix. The Kronecker product is denoted by $\otimes$ and $(\cdot)^H$ is the Hermitian operator. The matrix $\mathbf{X}_D$ is a $T^2NR\times P$ sparse matrix that contains the values α_l at the L indices (r_lTN+s_l,u_l).

Our goal is now to recover $\mathbf{X}_D$ from the measurement matrices $\mathbf{Z}^m, 0\le m\le M-1$. The time, spatial and frequency resolution stipulated by $\mathbf{X}_D$ are $\frac{1}{TB_h}$, $\frac{2}{TR}$ and $\frac{1}{P\tau}$ respectively. Theorem 1 presents necessary conditions on the minimal number of channels MQ, samples per receiver MK and pulses per transmitter P for perfect recovery of $\mathbf{X}_D$ from (10) under the grid assumption. The proof can be found in [15].

Theorem 1. *The minimal number of channels required for perfect recovery of $\mathbf{X}_D$ with L targets in noiseless settings is $MQ\ge 2L$ with a minimal number of $MK\ge 2L$ samples per receiver and $P\ge 2L$ pulses per transmitter.*

III-B. Range-Azimuth-Doppler Recovery

To recover jointly the range, azimuth and Doppler frequency of the targets, we apply the concept of Doppler focusing from [8] to our setting. Once the Fourier coefficients (9) are acquired and processed, we perform Doppler focusing for a specific frequency ν, that is

$$\begin{aligned}\Phi_{m,q}^{\nu}[k] &= \sum_{p=0}^{P-1} y_{m,q}^p[k]e^{-j2\pi\nu p\tau} \\ &= \sum_{l=1}^{L}\alpha_l e^{j2\pi\beta_{mq}\vartheta_l}e^{-j\frac{2\pi}{\tau}(k+f_m\tau)\tau_l}\sum_{p=0}^{P-1}e^{j2\pi(f_l^D-\nu)p\tau},\end{aligned} \tag{11}$$

for $-\frac{N}{2}\le k\le -\frac{N}{2}-1$. Following the same argument as in [8], it holds that

$$\sum_{p=0}^{P-1}e^{j2\pi(f_l^D-\nu)p\tau}\cong\begin{cases}P & |f_l^D-\nu|<\frac{1}{2P\tau},\\ 0 & otherwise.\end{cases} \tag{12}$$

Then, for each focused frequency ν, (11) reduces to a 2D problem.

Algorithm 1 extends orthogonal matching pursuit (OMP) to solve (10) using Doppler focusing. Note that step 1 can be performed using fast Fourier transform (FFT). In the algorithm description, vec($\mathbf{Z}$) concatenates the columns of $\mathbf{Z}^m$, $\mathbf{e}_t(l) = \left[(\mathbf{e}_t^0(l))^T\ \cdots\ (\mathbf{e}_t^{M-1}(l))^T\right]^T$ where $\mathbf{e}_t^m(l) = \text{vec}((\bar{\mathbf{B}}^m\otimes\mathbf{A}^m)_{\Lambda_t(l,2)TN+\Lambda_t(l,1)}\left((\bar{\mathbf{F}}^m)^T_{\Lambda_t(l,3)}\right)^T)$ with $\Lambda_t(l,i)$ the (l,i)th element in the index set Λ_t at the tth iteration, and $\mathbf{E}_t = [\mathbf{e}_t(1)\ldots\mathbf{e}_t(t)]$. Once $\mathbf{X}^p$ are recovered, the delays, azimuths and Dopplers are estimated as

$$\hat{\tau}_l = \frac{\tau\Lambda_L(l,1)}{TN},\ \hat{\vartheta}_l = -1+\frac{2\Lambda_L(l,2)}{TR},\ \hat{f}_l^D = -\frac{1}{2\tau}+\frac{\Delta_L(l,3)}{P\tau}. \tag{13}$$

III-C. Multi-Carrier SUMMeR

We now explain how the frequency bands left vacant can be exploited to increase the system's performance without expanding the total bandwidth of $B_{\text{tot}}=TB_h$. Denote by $\gamma=T/M$ the compression ratio of the number of transmitters. In this configuration, referred to as multi-carrier SUMMeR, each transmit antenna sends γ pulses in each PRI. Each pulse belongs to a different frequency band and are therefore mutually orthogonal, such that the total number of user bands is $M\gamma B_h = TB_h$. The ith pulse of the pth PRI is transmitted at time $i\frac{\tau}{\gamma}+p\tau$, for $0\le i<\gamma$ and $0\le p\le P-1$. The samples are then acquired and processed as described above. Besides increasing the detection performance as we show in simulations, this method multiplies the Doppler dynamic range by a factor of γ with the same Doppler resolution since the CPI, equal to $P\tau$, is unchanged. Preserving the CPI allows to maintain the targets' stationarity.

IV. SIMULATIONS

Throughout the experiments, the standard MIMO system is based on a virtual array, as depicted in Fig. 1(a), which would be generated by $T=20$ transmit antennas and $R=20$ receive antennas, yielding an aperture $\lambda Z = 6m$. The SUMMeR system is composed of $M<T$ transmitters and $Q<R$ receivers, with locations generated uniformly at random over the virtual array, as shown in Fig. 1(b). We use

Algorithm 1 OMP for simultaneous sparse 3D recovery with focusing

Input: Observation matrices $\mathbf{Z}^{(m,p)}$, measurement matrices $\mathbf{A}^{(m,p)}$, $\mathbf{B}^{(m,p)}$, for all $0 \leq m \leq M-1$ and $0 \leq p \leq P-1$

Output: Index set Λ containing the locations of the non zero indices of $\mathbf{X}$, estimate for sparse matrix $\hat{\mathbf{X}}$

1: Perform Doppler focusing for $0 \leq i \leq TN$ and $0 \leq j \leq TR$:

$$\mathbf{\Phi}_{i,j}^{(m,\nu)} = \sum_{p=0}^{P-1} \mathbf{Y}_{i,j}^{(m,p)} e^{j2\pi\nu p\tau}.$$

2: Initialization: residual $\mathbf{R}_0^{(m,p)} = \mathbf{\Phi}^{(m,p)}$, index set $\Lambda_0 = \emptyset$, $t = 1$

3: Project residual onto measurement matrices for $0 \leq p \leq P-1$:

$$\mathbf{\Psi}^p = \mathbf{A}^H \mathbf{R}^p \mathbf{B},$$

where $\mathbf{A} = [\mathbf{A}^{0^T}\ \mathbf{A}^{1^T} \cdots \mathbf{A}^{(M-1)^T}]^T$, $\mathbf{B} = [\mathbf{B}^{0^T}\ \mathbf{B}^{1^T} \cdots \mathbf{B}^{(M-1)^T}]^T$, and $\mathbf{R}^p = \text{diag}\left([\mathbf{R}_{t-1}^{(0,p)} \cdots \mathbf{R}_{t-1}^{(M-1,p)}]\right)$ is block diagonal

4: Find the three indices $\lambda_t = [\lambda_t(1)\, \lambda_t(2)\, \lambda_t(3)]$ such that

$$[\lambda_t(1) \quad \lambda_t(2) \quad \lambda_t(3)] = \arg\max_{i,j,\nu} \left|\mathbf{\Phi}_{i,j}^{\nu}\right|$$

5: Augment index set $\Lambda_t = \Lambda_t \bigcup \{\lambda_t\}$

6: Find the new signal estimate

$$\hat{\alpha} = [\hat{\alpha}_1 \ \ldots\ \hat{\alpha}_t]^T = (\mathbf{E}_t^T \mathbf{E}_t)^{-1} \mathbf{E}_t^T \text{vec}(\mathbf{Z})$$

7: Compute new residual

$$\mathbf{R}_t^{(m,p)} = \mathbf{Y}^m - \sum_{l=1}^{t} \alpha_l e^{j2\pi\left(-\frac{1}{2}+\frac{\Lambda_t(l,3)}{P}\right)p} \mathbf{a}^m_{\Lambda_t(l,1)} \left(\bar{\mathbf{b}}^m_{\Lambda_t(l,2)}\right)^T$$

8: If $t < L$, increment t and return to step 2, otherwise stop

9: Estimated support set $\hat{\Lambda} = \Lambda_L$

10: Estimated matrix $\hat{\mathbf{X}}_D$: $(\Lambda_L(l,2)TN + \Lambda_L(l,1), \Lambda_L(l,3))$-th component is given by $\hat{\alpha}_l$ while rest of the elements are zero

FDMA waveforms $h_m(t)$ such that $f_m = (i_m - \frac{T}{2})B_h$, where i_m are integers chosen uniformly at random in $[0, T]$, and with the following parameters: PRI $\tau = 100\mu sec$, bandwidth $B_h = 5MHz$ and carrier $f_c = 10GHz$. We consider targets from the Swerling-0 model with identical amplitudes and random phases. The received signals are corrupted with uncorrelated additive Gaussian noise with power spectral density N_0. We consider a hit-or-miss criterion as performance metric. A "hit" is defined as a range-azimuth-Doppler estimate which is identical to the true target position up to one Nyquist bin (grid point) defined as $1/TB_h$, $2/TR$ and $1/P\tau$ for the range azimuth and Doppler, respectively.

We first consider $L = 6$ targets including couples of targets with close ranges, azimuths and velocities, up to one grid point. We use $M = 10$ transmit antennas and $Q = 10$ receive antennas and employ $K = 250$ samples per channel instead of $N = B_h\tau = 500$, which corresponds to only 12.5% of the total number of Nyquist rate samples from the original array. The SNR is set to -10dB. Figure 4 shows the sparse target scene on a range-azimuth map, where each real target is displayed with its estimated location. The range and azimuth are converted to 2-dimensional x and y locations.

Next, we investigate the performance of our azimuth-range-Doppler recovery scheme with respect to SNR for different number of samples K per channel. We use the same array as described above, with spatial compression of 25%, where each transmitter sends $P = 10$ pulses,. We consider $L = 10$ targets whose locations are generated uniformly at random. Figure 5 presents the range-azimuth-Doppler recovery performance with respect to SNR. The configuration with $K = 500$ corresponds to samples obtained at the Nyquist rate and that with $K = 125$ is composed of only 6.25% of the total number of

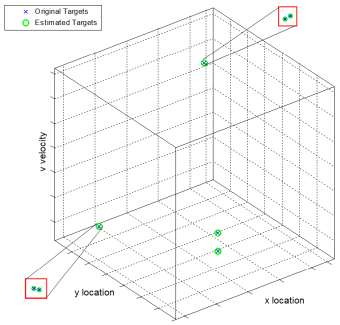

Fig. 4. Range-azimuth-Doppler recovery $L = 6$ targets and SNR=-10dB.

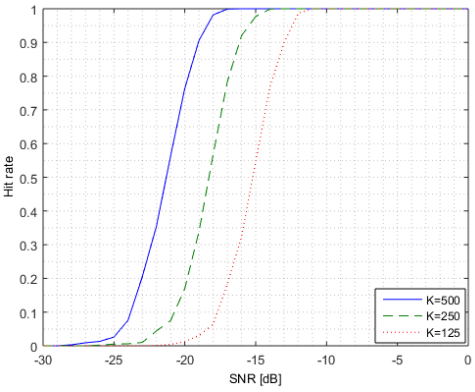

Fig. 5. Range-azimuth-Doppler recovery performance with time compression.

Nyquist rate samples from the original array. We observe a shift of 3dB between the consecutive graphs, since the compression between them yield a decrease of half the system power. Similar results are observed for spatial compression.

Last, we illustrate the increased detection performance achieved by the multi-carrier SUMMeR method. We consider the same system parameters as above with $L = 5$ targets. In the classic and SUMMeR system, $P = 10$ pulses are transmitted by each transmit antenna. In multi-carrier SUMMeR, we have $\gamma = 2$, leading to $2P = 20$ pulses per transmitter. In Fig. 6, we observe that the multi-carrier approach with spatial compression achieves the same performance as the original SUMMeR and the classic processing with no compression. The reduction of the number of receivers decreases the performance by 3dB, which are compensated by the extra transmitted pulses.

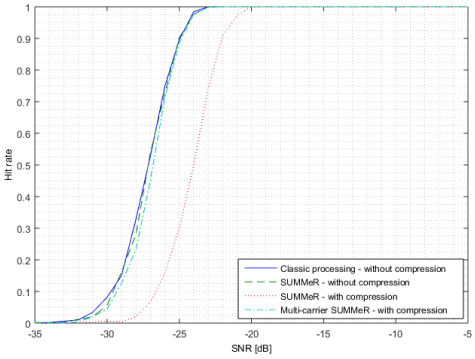

Fig. 6. Multi-carrier SUMMeR with spatial compression.

V. REFERENCES

[1] E. Fishler, A. Haimovich, R. Blum, D. Chizhik, L. Cimini, and R. Valenzuela, "MIMO radar: an idea whose time has come," in *IEEE Radar Conf.*, 2004, pp. 71–78.

[2] J. Li and P. Stoica, "MIMO radar with collocated antennas," *IEEE Signal Process. Magazine*, vol. 24, no. 5, pp. 106–114, 2007.

[3] ——, "Mimo radar - diversity means superiority," in *Adaptive Sensor Array Process. Workshop*, 2009, pp. 1–6.

[4] M. Rossi, A. M. Haimovich, and Y. C. Eldar, "Spatial compressive sensing for MIMO radar," *IEEE Trans. Signal Process.*, vol. 62, no. 2, pp. 419–430, 2014.

[5] Y. Yu, A. P. Petropulu, and H. V. Poor, "MIMO radar using compressive sampling," *IEEE J. Sel. Topics Signal Process.*, vol. 4, no. 1, pp. 146–163, 2010.

[6] D. S. Kalogerias and A. P. Petropulu, "Matrix completion in colocated MIMO radar: Recoverability, bounds & theoretical guarantees," *IEEE Trans. Signal Process.*, vol. 62, no. 2, pp. 309–321, 2014.

[7] S. Sun, W. U. Bajwa, and A. P. Petropulu, "MIMO-MC radar: A MIMO radar approach based on matrix completion," *CoRR*, vol. abs/1409.3954, 2014. [Online]. Available: http://arxiv.org/abs/1409.3954

[8] O. Bar-Ilan and Y. C. Eldar, "Sub-Nyquist radar via Doppler focusing," *IEEE Trans. Signal Process.*, vol. 62, no. 7, pp. 1796–1811, 2014.

[9] M. Mishali, Y. C. Eldar, O. Dounaevsky, and E. Shoshan, "Xampling: Analog to digital at sub-Nyquist rates," *IET circuits, Devices & Systems*, vol. 5, no. 1, pp. 8–20, 2011.

[10] E. Baransky, G. Itzhak, I. Shmuel, N. Wagner, E. Shoshan, and Y. C. Eldar, "A sub-Nyquist radar prototype: Hardware and applications," *IEEE Trans. Aerosp. and Elect. Syst.*, vol. 50, pp. 809–822, Apr. 2014.

[11] C.-Y. Chen, "Signal processing algorithms for MIMO radar," Ph.D. dissertation, California Institute of Technology, 2009.

[12] P. Z. Peebles, *Radar principles*. John Wiley & Sons, 2007.

[13] P. Vaidyanathan, P. Pal, and C.-Y. Chen, "MIMO radar with broadband waveforms: Smearing filter banks and 2D virtual arrays," *Asilomar Conf. Signals, Syst. and Computers*, pp. 188–192, 2008.

[14] M. Skolnik, *Radar handbook*. McGraw Hill, 1970.

[15] D. Cohen, D. Cohen, Y. C. Eldar, and A. M. Haimovich, "SUMMeR: sub-Nyquist MIMO radar," 2016.